Geophysical Prospecting, 2003, **51**, 141–157

Acoustic properties of sediments saturated with gas hydrate, free gas and water

Davide Gei and José M. Carcione*

Istituto Nazionale di Oceanografia e di Geofisica Sperimentale (OGS), Borgo Grotta Gigante 42C, 34010 Sgonico, Trieste, Italy

Received January 2002, revision accepted November 2002

ABSTRACT

We obtain the wave velocities and quality factors of gas-hydrate-bearing sediments as a function of pore pressure, temperature, frequency and partial saturation. The model is based on a Biot-type three-phase theory that considers the existence of two solids (grains and gas hydrate) and a fluid mixture. Attenuation is described with the constant-Q model and viscodynamic functions to model the high-frequency behaviour. We apply a uniform gas/water mixing law that satisfies Wood's and Voigt's averages at low and high frequencies, respectively. The acoustic model is calibrated to agree with the patchy-saturation theory at high frequencies (White's model). Pressure effects are accounted by using an effective stress law for the dry-rock moduli and permeabilities. The dry-rock moduli of the sediment are calibrated with data from the Cascadia margin. Moreover, we calculate the depth of the bottom simulating reflector (BSR) below the sea floor as a function of sea-floor depth, geothermal gradient below the sea floor, and temperature at the sea floor.

1 INTRODUCTION

Gas hydrate is a clathrate composed of water and natural gas, mainly methane, which forms under conditions of low temperature, high pressure, and proper gas concentration. Bottom simulating reflectors (BSRs) on seismic profiles are interpreted as representing the seismic signature of the base of gas-hydrate formation; a free gas zone may be present just below the BSR (e.g. Andreassen, Hogstad and Berteussen 1990). Where no direct measurements are available, detailed knowledge of the seismic properties is essential for quantitative estimations of gas hydrate and free gas in the pore space (Tinivella and Carcione 2001).

Wave velocities and attenuation are two important properties which can give information about lithology, saturation, and the *in situ* conditions of rocks. It is therefore important to obtain a relationship between these properties and gas-hydrate concentration, porosity, pore and confining pressures, frequency, and gas and water saturation. Carcione and Tinivella (2000) modelled the acoustic properties of gas-hydrate-bearing sediments saturated with water in the framework of Biot's theory of poroelasticity. Unlike previous theories, Carcione and Tinivella's (2000) approach uses a Biot-type three-phase theory that considers the existence of two solids (grains and gas hydrate) and water. The theory is generalized here to include the effects of pore pressure, partial saturation (gas and water) and the presence of dissipation mechanisms of different nature. The coexistence of the three phases in the pore space (gas hydrate, free gas and water) has been justified by Xu and Ruppel (1999). Although thermodynamic conditions dictate that only two phases should be present, in systems undergoing rapid phase changes the three phases may coexist. Moreover, observational data (ODP Leg 164, Paull *et al.* 1996; Guerin, Goldberg and Meltser 1999) indicate that the three phases probably coexist within the hydrate stability zone.

Pressure effects are introduced by using an effective stress law. As is well known, at constant effective pressure the acoustic (or transport) properties of the rock remain constant. The effective pressure depends on the difference between the confining and pore pressures, the latter multiplied by the effective stress coefficient. In general, this coefficient is

*E-mail: jcarcione@ogs.trieste.it

not equal to one and, therefore, the Terzaghi effective pressure law (that is, effective pressure equal to differential pressure) is not an appropriate quantity to describe the acoustic properties of the rock under varying pore pressure.

The effect of partial saturation on velocity and attenuation depends on the frequency range. At low frequencies, the fluid has enough time to achieve pressure equilibration (relaxed regime). In this case, Wood's model for the bulk modulus of the fluid mixture yields results that agree with the experiments. On the other hand, at high frequencies the fluid cannot relax and this unrelaxed state induces a stiffening of the pore material, which increases the wave velocity considerably (Cadoret, Marion and Zinszner 1995). This effect implies an uneven distribution of fluids in the pore space, which is normally termed patchy saturation. In this case, Wood's model is not appropriate and, in general, a Hill average is used to model the wave velocities at ultrasonic (laboratory) frequencies (Dvorkin *et al.* 1999; Johnson 2001). No microstructural theory is able to predict the behaviour at intermediate frequencies. In the present model, we use a modified empirical fluid mixing law proposed by Brie *et al.* (1995), which gives Wood's modulus at low frequencies and Voigt's modulus at high frequencies.

Attenuation is described by using a constant-Q model for the dry-rock moduli (Kjartansson 1979; Carcione *et al.* 2002). This approach is phenomenological, since a theory describing all the attenuation mechanisms present in a real rock is difficult, if not impossible, to develop. The constant-Q kernel is the most simple model based on only one parameter. We assume that the lower the frame modulus, the lower the quality factor (that is, the higher the attenuation). Using this property, we assign a Q-factor to the frame bulk modulus, and obtain the Q-factor associated with the shear modulus. The attenuation mechanisms predicted by the low-frequency Biot theory (1962) are modelled by the original theory (Carcione and Tinivella 2000), and, here, we introduce high-frequency viscodynamic effects, based on an optimal viscodynamic function obtained by Johnson, Koplik and Dashen (1987).

The acoustic model developed by Carcione and Tinivella (2000) yields the seismic velocities as a function of gas-hydrate concentration, porosity, saturation, dry-rock moduli, and fluid and solid-grain properties. As stated in previous works (Carcione and Gangi 2000a, b), the large change in seismic velocity is mainly due to the fact that the dry-rock moduli are sensitive functions of the effective pressure, with the largest changes occurring at low differential pressures. The major effect of porosity changes is implicit in the dry-rock moduli. Changes in porosity and saturation are important but have a lesser influence than changes in the moduli. In this sense, porosity-based methods can be highly unreliable. In fact, variations of porosity for Navajo sandstone (11.8%), Weber sandstone (9.5%) and Berea sandstone (17.8%) are only 0.2%, 0.7% and 0.8% porosity units, respectively, for changes in the confining pressure from 0 to 100 MPa, while the corresponding increases in bulk moduli are in the range 15–20 GPa (Coyner 1984; Berryman 1992). To obtain the expression of the dry-rock moduli versus effective pressure, the model requires calibration based on well, geological and laboratory data, mainly sonic and density data, and porosity and gas-hydrate concentration inferred from logging profiles.

Before discussing the acoustic properties we provide a simple model of gas-hydrate stability, i.e. how to calculate the depth of the BSR below the sea floor as a function of sea-floor depth, geothermal gradient below the sea floor, and temperature at the sea floor. This calculation is performed for several ODP sites. Site 892 is used to illustrate the acoustic theory, since laboratory measurements are available for calibration (MacKay *et al.* 1994; Tobin, Moore and Moore 1995).

2 METHANE HYDRATE STABILITY: BSR POSITION VERSUS DEPTH

On continental margins, knowledge of pore pressure, temperature and geothermal gradient is necessary to determine the base of the hydrate stability field. Dickens and Quinby-Hunt (1994) presented experimental data for methane hydrate stability conditions in seawater. The following empirical equation for the dissociation temperature, obtained by Peltzer and Brewer (2000), fits the data fairly well:

$$\frac{1}{T} = a + b\log p + c(\log p)^2, \tag{1}$$

where T is temperature (in kelvin), p is pore pressure (in MPa), and $a = 3.83 \times 10^{-3}$, $b = -4.09 \times 10^{-4}$ and $c = 8.64 \times 10^{-5}$, for a salinity of 33.5 ppt and a pressure range of 2.5–10 MPa.

Let us assume a temperature T_0 and a pressure p_0 at the sea floor. The hydrostatic pore pressure is $p_0 = \rho_w g z_0$, where ρ_w is the density of water, z_0 is the depth of the sea floor, and g is the acceleration of gravity. For a constant geothermal gradient G, the temperature variation below the sea floor is

$$T = T_0 + G(z - z_0), \tag{2}$$

where z is the depth. Typical values of G range from 0.03 to 0.1 °C/m (Grevemeyer and Villinger 2001). A linear

relationship for the hydrostatic pore pressure below the sea floor is given by

$$p = p_0 + \rho_w g(z - z_0) = \rho_w g z, \quad (3)$$

because $p_0 = \rho_w g z_0$. We do not account for variations in water density with p and T and variations in g with latitude and longitude. The difference is small (approximately 10 m for a latitude of 30° and $p = 10$ MPa) (Fofonoff and Millard 1982). Substituting (2) and (3) into (1) gives the depth of the BSR.

Brown and Bangs (1995) fitted the data of Dickens and Quinby-Hunt (1994) to a different polynomial:

$$T = T_0 + G(z - z_0) = 11.726 + 20.5 \log z - 2.2[\log z]^2, \quad (4)$$

where T is given in °C and z in km (see also Peltzer and Brewer 2000; they used 11.726 instead of 11.66 reported by Brown and Bangs 1995). The two curves differ when extrapolated to higher p–T conditions, but there is no conclusive evidence of the behaviour of the data at high p–T conditions. Only one data set for seawater exists, and it is limited to pure methane gas measurements (Peltzer and Brewer 2000). The equations can be solved for z with a Newton–Raphson method.

Figure 1 shows the depth of the BSR for different sites. This depth is given by the intersection between the black curve (equation (1)) and the dotted line (equation (2)). The measured data are indicated by asterisks. The grey line corresponds to Brown and Bangs's (1995) curve (4). The upper horizontal line indicates the sea floor. As can be appreciated, Peltzer and Brewer's (2000) equation provides the best approximation.

Let us consider site 892, for which $\rho_w = 1040$ kg/m^3, $T_0 = 4.05$ °C, $g = 9.8$ m/s^2, $z_0 = 748$ m and $G = 0.0694$ °C/m (Grevemeyer and Villinger 2001). Figure 2 shows the position of the BSR as a function of (a) the geothermal gradient G, (b) the depth of the sea floor z_0, and (c) the sea-floor temperature T_0. The BSR position is deeper for lower geothermal gradients. Moreover, it is more sensitive than for high geothermal gradients. The depth of the BSR increases with increasing depth and decreasing temperature of the sea floor.

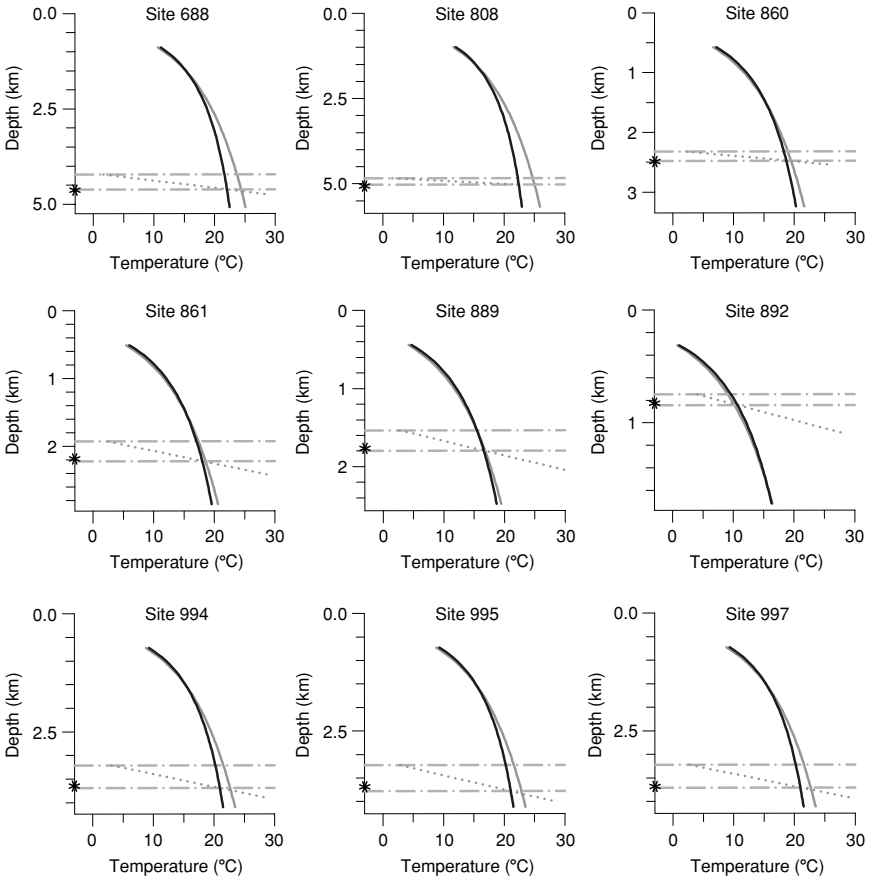

Figure 1 The intersection of the geothermal-gradient line (dotted line; see equation (2)) and the curve (1) (black line) gives the depth of the BSR (lower horizontal line). The measured data are indicated by asterisks. The grey line corresponds to Brown and Bangs's curve (4). The upper horizontal line indicates the sea floor. Data are from ODP Legs 112 (Suess *et al.* 1988), 131 (Taira *et al.* 1991), 141 (Behrmann *et al.* 1992), 146 (Westbrook *et al.* 1994; Davis *et al.* 1995) and 164 (Paull *et al.* 1996). The complete data set for each site is given in Grevemeyer and Villinger (2001) (their table 1).

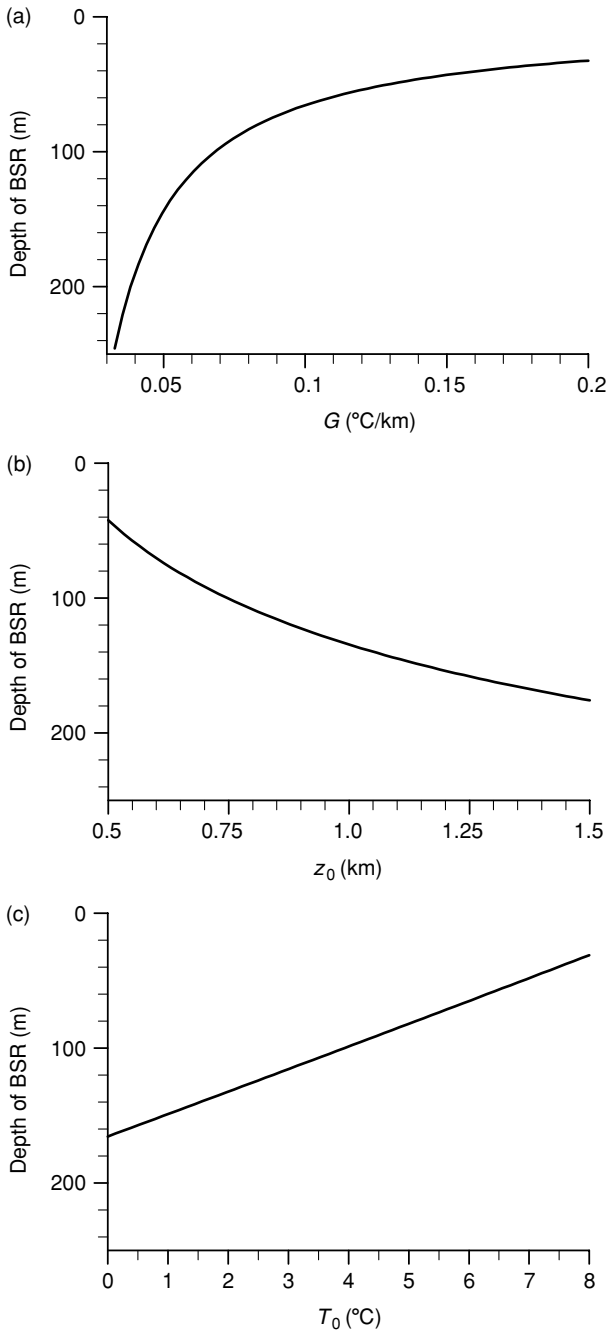

Figure 2 Position of the BSR below the sea floor as a function of (a) the geothermal gradient G, (b) the depth of the sea floor z_0, and (c) the sea-floor temperature T_0.

3 THE ACOUSTIC MODEL

The model, developed by Carcione and Tinivella (2000) and based on the theory of Leclaire, Cohen-Ténoudji and Aguirre-Puente (1994), takes explicitly into account the presence of three phases: grains, gas hydrate and fluid. The input quantities that play a role in the generalization to include pressure, attenuation and saturation effects are:

- the solid-grain fraction, ϕ_s,
- the gas-hydrate fraction, ϕ_h,
- the water fraction, ϕ_w,
- the gas fraction, ϕ_g,
- the porosity, $\phi = \phi_h + \phi_w + \phi_g$,
- the water saturation, $S_w = \phi_w/(\phi_w + \phi_g)$,
- the gas saturation, $S_g = \phi_g/(\phi_w + \phi_g)$,
- the bulk modulus of the rock frame (without hydrate), K_{sm},
- the shear modulus of the rock frame (without hydrate), μ_{sm},
- the fluid-mixture bulk modulus, K_f,
- the fluid-mixture viscosity, η_f,
- the tortuosity of the fluid mixture flowing through the rock frame, $\mathcal{T}_1$ (a_{12} in Carcione and Tinivella 2000),
- the tortuosity of the fluid mixture flowing through the gas-hydrate matrix, $\mathcal{T}_3$ (a_{23} in Carcione and Tinivella 2000),
- the rock-frame permeability in the absence of gas hydrate, κ_{s0},
- the permeability of the gas-hydrate matrix in the absence of fluid, κ_{h0},
- the friction coefficient between the rock frame and the fluid, b_{11},
- the friction coefficient between the gas-hydrate matrix and the fluid, b_{33}.

The following relationship holds:

$$\phi_s + \phi_h + \phi_w + \phi_g = 1. \tag{5}$$

Water, gas and gas hydrate fill the pore volume, represented by the porosity ϕ. Use of the equations of Carcione and Tinivella (2000) requires the substitution of ϕ_w by $\phi_w + \phi_g$, K_w by K_f, ρ_w by ρ_f and η_w by η_f. (Note an omission in equations (B2), (B3) and (B4) of Carcione and Tinivella (2000): the term K_{sm} has to be added to K_1 and K_{im} (K_{hm} here) to K_3.)

4 PORE PRESSURE AND DRY-ROCK MODULI

The theory needs calibration either with log data or with laboratory data, as described in the following sections.

4.1 Calibration with log data

We consider the model of Krief *et al.* (1990) to obtain an estimation of the dry-rock moduli K_{sm}, μ_{sm} (frame), and K_{hm} and μ_{hm} (gas-hydrate matrix) versus porosity and gas-hydrate

content. The porosity dependence of the rock frame and gas-hydrate matrix should be consistent with the concept of critical porosity, since the moduli should be small above a certain value of the porosity (usually from 0.4 to 0.6) (e.g. Guerin *et al.* 1999). This dependence is determined by the empirical coefficient A (see (6)). This relationship was suggested by Krief *et al.* (1990) and applied to sand/clay mixtures by Goldberg and Gurevich (1998). The bulk and shear moduli of the rock frame and gas-hydrate matrix are respectively given by

$$\begin{aligned} K_{\mathrm{sm}}(z) &= \phi_{\mathrm{s}}(z) K_{\mathrm{s}} [1 - \phi(z)]^{A/[1-\phi(z)]}, \\ K_{\mathrm{hm}}(z) &= \phi_{\mathrm{h}}(z) K_{\mathrm{h}} [\phi_{\mathrm{h}}(z)]^{A/\phi_{\mathrm{h}}(z)}, \\ \mu_{\mathrm{sm}}(z) &= K_{\mathrm{sm}}(z) \mu_{\mathrm{s}} / K_{\mathrm{s}}, \\ \mu_{\mathrm{hm}}(z) &= K_{\mathrm{hm}}(z) \mu_{\mathrm{h}} / K_{\mathrm{h}}, \end{aligned} \tag{6}$$

where K_{s} and μ_{s} are the bulk and shear moduli of the grains, and K_{h} and μ_{h} are those of the gas-hydrate particles. Krief *et al.* (1990) set the A parameter to 3 regardless of the lithology, and Goldberg and Gurevich (1998) obtained values between 2 and 4. Alternatively, the value of A can be estimated by using regional data from the study area.

We assume the following functional form for the dry-rock moduli as a function of depth and effective pressure:

$$\begin{aligned} K_{\mathrm{sm}}(z, p) &= \beta K_{\mathrm{HS}} [1 - \exp(-p_{\mathrm{e}}(p) / p^*_K(z))], \\ \mu_{\mathrm{sm}}(z, p) &= \beta \mu_{\mathrm{HS}} [1 - \exp(-p_{\mathrm{e}}(p) / p^*_\mu(z))], \end{aligned} \tag{7}$$

where $p^*(z)$ is obtained (for each modulus) by fitting Krief *et al.*'s (1990) expressions (6), and β is an empirical coefficient (see below). The effective pressure at depth z is assumed to be $p_{\mathrm{e}} = p_{\mathrm{c}} - np$, where p_{c} is the confining pressure, p is the pore pressure and n is the effective stress coefficient, which can be assumed equal to 1 (Zimmerman 1991, p. 43). (Alternatively, the effective stress coefficients can be estimated from sonic-log information and direct pressure measurements (if available) by fitting the theoretical velocities to the experimental velocities.) Moreover, K_{HS} and μ_{HS} are the Hashin–Shtrikman (HS) upper bounds (Hashin and Shtrikman 1963; Mavko, Mukerji and Dvorkin 1998, p. 106). The Voigt bounds are $(1 - \phi)K_{\mathrm{s}}$ and $(1 - \phi)\mu_{\mathrm{s}}$, respectively. For quartz grains with gas hydrate, $K_{\mathrm{s}} = 39$ GPa and $\mu_{\mathrm{s}} = 33$ GPa (Mavko *et al.* 1998, p. 307), and if the porosity is 0.2, the HS upper bounds for the bulk and shear moduli are 26 GPa and 22 GPa, compared with the Voigt upper bounds 31 GPa and 26 GPa, respectively. However, the HS bounds are too large to model the moduli of *in situ* rocks. These contain clay and residual water saturation, inducing a chemical weakening of the contacts between grains (Knight and Dvorkin 1992; Mavko *et al.* 1998, p. 203). Therefore, these bounds are multiplied by the parameter β, which can be obtained by fitting regional data.

4.2 Calibration with laboratory data

An alternative and more precise evaluation of the dry-rock moduli can be obtained from laboratory experiments. The seismic bulk and shear moduli K_{sm} and μ_{sm}, respectively, versus confining pressure can be obtained from laboratory measurements in dry and saturated samples (see Section 8). The moduli of the matrix formed by gas hydrate are obtained from the percolation model described by Leclaire *et al.* (1994) and Carcione and Tinivella (2000). The effective stress coefficients can be measured in the laboratory from experiments on wet-rock samples versus confining and pore pressures. In this way, the effective pressure law can be obtained. When using laboratory experiments to determine n, we should keep in mind that this 'laboratory' n does not reflect the behaviour of the rock in the *in situ* conditions, due to two main reasons. First, laboratory measurements of wave velocity are performed at ultrasonic frequencies, and, therefore, the 'seismic' and 'laboratory' n's should be different. Second, the *in situ* stress distribution is different from the stress applied in the experiments. In this sense, log data should provide a better evaluation of the effective stress coefficients.

The evaluation of the dry-rock moduli and n from wet-rock velocities is illustrated in the example.

5 EFFECTIVE FLUID MODEL FOR PARTIAL SATURATION

The mixture free gas/water behaves as a composite fluid with properties depending on the constants of the constituents and their relative concentrations. The modulus and density are

$$K_{\mathrm{f}} = (S_{\mathrm{g}} K_{\mathrm{g}}^{-1} + S_{\mathrm{w}} K_{\mathrm{w}}^{-1})^{-1} \tag{8}$$

(Wood's model) and

$$\rho_{\mathrm{f}} = S_{\mathrm{g}} \rho_{\mathrm{g}} + S_{\mathrm{w}} \rho_{\mathrm{w}}, \tag{9}$$

where K_{w} and K_{g} are the water and gas bulk moduli, and ρ_{w} and ρ_{g} are the respective densities. Moreover, the fluid viscosity is

$$\eta_{\mathrm{f}} = \eta_{\mathrm{g}} \left(\frac{\eta_{\mathrm{w}}}{\eta_{\mathrm{g}}} \right)^{S_{\mathrm{w}}} \tag{10}$$

(Teja and Rice, 1981a, b), where η_g and η_w are the viscosities of the free gas and water, respectively. Equation (10) is a good approximation for most values of the saturations. In the examples, we compare this equation to the linear law $\eta_f = S_w \eta_w + S_g \eta_g$.

Equation (8) corresponds to the low-frequency range. When the fluids are not mixed in the pore volume, but distributed in patches, the effective bulk modulus of the fluid at high frequencies is higher than that predicted by (8). We use an empirical mixing law introduced by Brie *et al.* (1995). The effective fluid bulk modulus is given by

$$K_f = (K_w - K_g)(S_w)^e + K_g, \tag{11}$$

where $e = (f_0/f)^{0.36}$ is an empirical parameter, with f_0 being a reference frequency. The exponent 0.36 fits data from the seismic to the ultrasonic band, particularly, the sonic-band values provided by Brie *et al.* (1995). As shown later, the reference frequency is chosen such that the model fits the Hill average at 1 MHz. Equation (11) gives Voigt's mixing law for $e = 1$ and Wood's model for $e = 40$.

The isothermal gas bulk modulus K_g and the gas compressibility $c_g = {K_g}^{-1}$ depend on pressure. The latter can be calculated from the van der Waals equation,

$$(p + a\rho_g^2)(1 - b\rho_g) = \rho_g RT, \tag{12}$$

where p is the gas pressure, ρ_g is the gas density, T is the absolute temperature and R is the gas constant. Moreover, a good approximation can be obtained using $a = 0.225$ Pa $(\mathrm{m^3/mole})^2 = 879.9$ MPa $(\mathrm{cm^3/g})^2$ and $b = 4.28 \times 10^{-5}\ \mathrm{m^3/mole} = 2.675\ \mathrm{cm^3/g}$ (one mole of methane, CH_4, corresponds to 16 g). Then,

$$c_g = \frac{1}{\rho_g}\frac{\mathrm{d}\rho_g}{\mathrm{d}p} = \left[\frac{\rho_g RT}{(1 - b\rho_g)^2} - 2a\rho_g^2\right]^{-1}. \tag{13}$$

We assume that the viscosity of water is independent of pressure.

The gas (methane) viscosity is that proposed by Luo and Vasseur (1996). It depends on pore pressure and temperature T:

$$\eta_g\ [\mathrm{Pa.s}] = 10^{-5} + 1.5 \times 10^{-8}\left(\frac{p}{\bar{\rho} g}\right) - 2.2 \times 10^{-7}(T - T_0), \tag{14}$$

where T_0 is the surface temperature and $\bar{\rho}$ is the average density of the overburden.

6 PERMEABILITY, PORE PRESSURE AND PARTIAL SATURATION

The permeabilities of the frame and gas-hydrate matrix versus pore and confining pressure can be obtained by multiplying κ_{s0} and κ_{h0} by the factor $[1 - (p_d/p_1)^m]^3$, i.e.

$$\kappa_s = \kappa_{s0}\left[1 - \left(\frac{p_d}{p_1}\right)^m\right]^3 \quad \text{and} \quad \kappa_h = \kappa_{h0}\left[1 - \left(\frac{p_d}{p_1}\right)^m\right]^3, \tag{15}$$

where $p_d = p_c - p$ is the differential pressure and p_1 and m are constants. This pressure dependence is due to Gangi (1981) and we have assumed that effective stress coefficients for permeability are equal to 1.

For a partially saturated medium, the permeabilities are further multiplied by the factor

$$\kappa_{rw} S_w + \kappa_{rg} S_g, \tag{16}$$

where κ_{rw} and κ_{rg} are normalized relative permeabilities given by

$$\kappa_{rw} = \sqrt{S_{we}}[1 - (1 - S_{we}^{1/m_w})^{m_w}]^2, \quad S_{we} = \frac{S_w - S_{wg}}{1 - S_{wg}}, \tag{17}$$

and

$$\kappa_{rg} = \sqrt{S_{ge}}[1 - (1 - S_{ge}^{1/m_g})^{m_g}]^2, \quad S_{ge} = \frac{S_g - S_{gw}}{1 - S_{gw}} \tag{18}$$

(Van Genuchten 1978; Bear and Bachmar 1990, p. 360). In (17) and (18), S_{gw} and S_{wg} are residual saturations of water in gas and gas in water, respectively, and we set $m_w = 0.8$ for water and $m_g = 1.8$ for gas.

7 ATTENUATION AND VISCODYNAMIC EFFECTS

Constant-Q models provide a simple parametrization of seismic attenuation in rocks in oil exploration and in seismology. By reducing the number of parameters they allow an improvement of seismic inversion. Moreover, there is physical evidence that attenuation is almost linear with frequency (therefore Q is constant) in many frequency bands. Bland (1960) and Kjartansson (1979) discussed a linear attenuation model with the required characteristics, but the idea is much older (Scott-Blair 1949).

The attenuation kernel corresponding to a constant Q over all frequencies is

$$M(\omega, Q) = \left(\frac{\mathrm{i}\omega}{\omega_0}\right)^{2\gamma}, \quad \gamma = \frac{1}{\pi}\tan^{-1}\left(\frac{1}{Q}\right), \tag{19}$$

where ω_0 is a reference frequency. Attenuation is modelled by

making the frame bulk and shear moduli viscoelastic. Then,

$$K_{sm} \rightarrow K_{sm} M(\omega, Q_K), \tag{20}$$

where

$$Q_K = \frac{K_{sm}(z,p)}{K_{sm}(z)} Q_0, \tag{21}$$

where Q_0 is the loss parameter of the frame and $K_{sm}(z)$ is the bulk modulus at full water saturation and hydrostatic pore pressure. The corresponding Q factors for the shear modulus are given by

$$Q_\mu = \frac{\mu_{sm}(z,p)}{K_{sm}(z,p)} Q_K \tag{22}$$

and

$$\mu_{sm} \rightarrow \mu_{sm} M(\omega, Q_\mu). \tag{23}$$

Equation (22) implies that the lower the modulus the higher the attenuation. Equations (21) and (22) should be considered with caution, since for unconsolidated sediments (suspensions) the bulk and shear moduli of the frame are zero. In this case, the attenuation can be described by the theory of sound absorption in suspensions (e.g. Urick 1948; McCann 1969). Our model implies that attenuation decreases with increasing hydrate concentration. Guerin and Goldberg (2002) observed the opposite behaviour in sonic waveforms. They used the viscodynamic operator developed by Leclaire *et al.* (1994) to qualitatively explain this effect. In our case, the inclusion of a medium stiffer than water (hydrate) and grain cementation with increasing hydrate content makes the porous medium more cohesive and attenuation should decrease. Viscodynamic effects of the Biot type, similar to Leclaire *et al.*'s (1994) formulation, are described below.

The introduction of high-frequency viscodynamic effects implies

Table 1 Material properties of the gas-hydrate-bearing sediment (e.g. Mavko *et al.* 1998). The values for the gas properties correspond to the depth of the BSR of site 892 (hydrostatic pore pressure)

Solid grain	Bulk modulus, K_s	35 GPa
	Shear modulus, μ_s	35 GPa
	Density, ρ_s	2650 kg/m^3
Gas hydrate*	Bulk modulus, K_h	7.9 GPa
	Shear modulus, μ_h	3.3 GPa
	Density, ρ_h	900 kg/m^3
Fluids	Bulk modulus, K_w	2.4 GPa
	Density, ρ_w	1030 kg/m^3
	Viscosity, η_w	1.798 cP
	Bulk modulus, K_g	7 MPa
	Density, ρ_g	70 kg/m^3
	Viscosity, η_g	0.021 cP

*Helgerud *et al.* (1999).

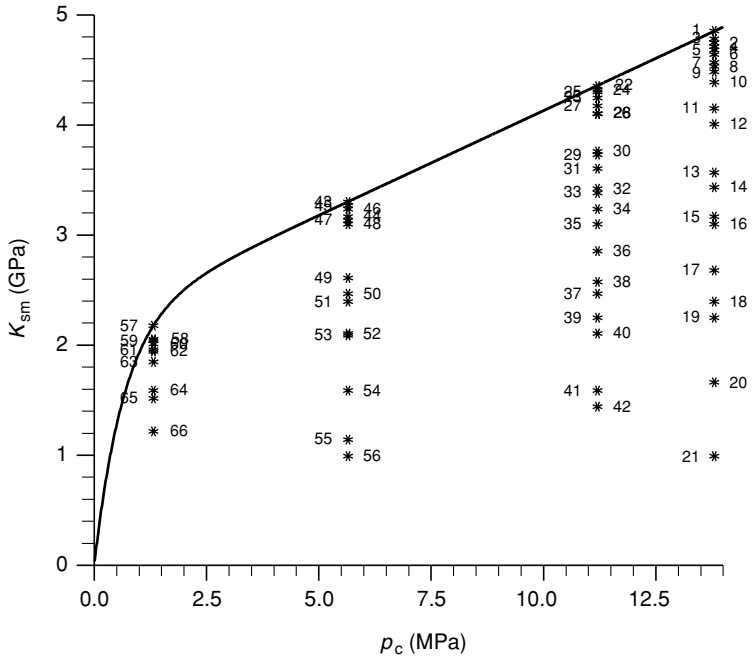

Figure 3 Dry-rock bulk modulus at zero pore pressure versus confining pressure (solid line). The stars correspond to the dry-rock moduli obtained by using (28) and the experimental data of Tobin *et al.* (1995).

$$b_{ii} = \left[\frac{\eta_f(\phi_w + \phi_g)^2}{\kappa_i}\right] F_i(\omega), \quad i = 1, 3, \tag{24}$$

where F_1 and F_3 are viscodynamic functions corresponding to the interaction between the rock frame and gas-hydrate matrix with the fluids, and $\kappa_1 = \kappa_s$ and $\kappa_3 = \kappa_h$ (Biot 1962). Johnson *et al.* (1987) obtained an expression for the viscodynamic function, which provides a good description of both the magnitude and phase of the exact dynamic tortuosity of large networks formed from a distribution of random radii (see also Carcione 2001, p. 252). The viscodynamic functions can be expressed as

$$F_i(\omega) = \sqrt{1 - \frac{4i\mathcal{T}_i^2\kappa_i}{x_i L_i^2(\phi_w + \phi_g)}}, \quad x_i = \frac{\eta_f(\phi_w + \phi_g)}{\omega\kappa_i\rho_f}, \quad i = 1, 3, \tag{25}$$

where L_i is a geometrical parameter, with $2/L_i$ being the surface-to-pore volume ratio of the pore–solid interface. The following relationship between $\mathcal{T}_i$, κ_i and L_i can be used: $\xi_i\mathcal{T}_i\kappa_i/(\phi_w + \phi_g)\ {L_i}^2 = 1$, where ξ_i describes the shape of the pore network; $\xi_i = 12$ for a set of canted slabs of fluid, and $\xi_i = 8$ for a set of non-intersecting canted tubes.

8 EXAMPLE

We use laboratory measurements to calibrate the theory, i.e. to obtain the properties of the dry rock as a function of pore and confining pressure. Effective stress and effective pressure play an important role in rock physics. The use of this concept is motivated by the fact that pore pressure and confining pressure tend to have opposite effects on the acoustic and transport properties of the rock. Thus, it is convenient to characterize those properties with a single pressure, the effective pressure. First, we obtain the dry-rock moduli versus confining pressure (zero pore pressure). Then, we obtain the effective stress coefficients and replace the confining pressure by the effective pressure. This constitutes the effective pressure law.

We consider water-saturated sediments of the Oregon accretionary prism (clayey silts). Tobin *et al.* (1995) performed laboratory experiments for wave velocity versus confining and pore pressure. We chose the sample 146-892D-18X-2, 0–22 cm from site 892 (their fig. 5b). Since only P-wave velocity is available, we assume the V_P to V_S relationships reported by Hamilton (1979) for 20 areas, consisting of silt clays, turbidites and mudstones:

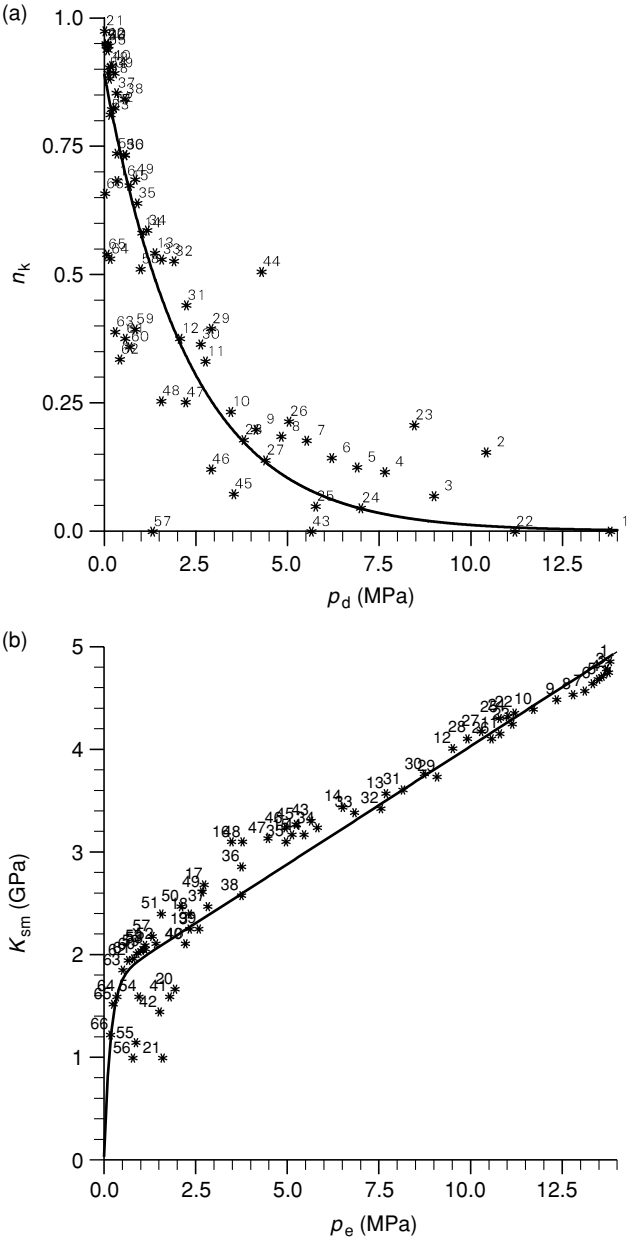

Figure 4 (a) Effective stress coefficients and corresponding exponential fit (solid line) versus differential pressure, and (b) dry-rock bulk modulus versus effective pressure.

$$\begin{aligned} &1650\ \text{m/s} < V_P < 2150\ \text{m/s} \\ &\quad V_S = 0.991 - 1.136V_P + 0.47V_P^2, \\ &V_P > 2150\ \text{m/s} \quad V_S = 0.78V_P - 0.962. \end{aligned} \tag{26}$$

For each data point in fig. 5(b) of Tobin *et al.* (1995), we compute the wet-rock bulk modulus as

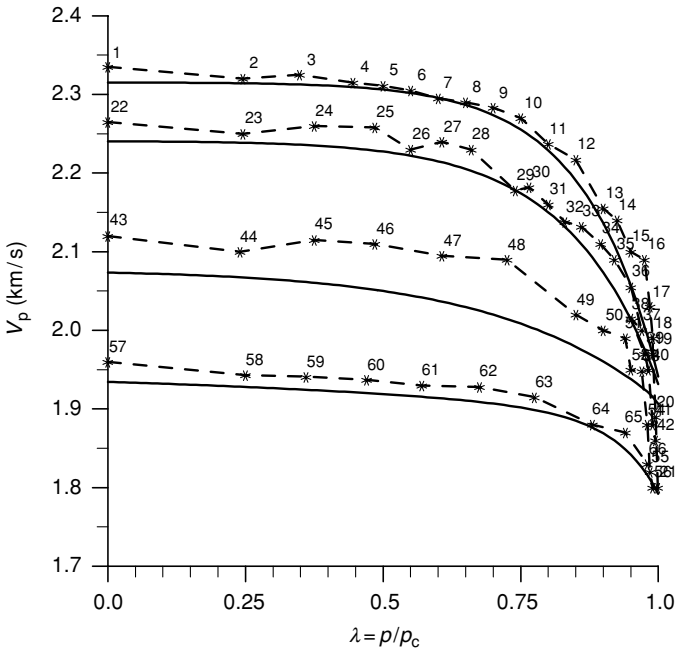

Figure 5 P-wave velocities versus overpressure ratio obtained with the effective pressure law (solid curves). The original data points of Tobin *et al.* (1995) are represented, where the confining pressures corresponding to the dashed curves are 13.8, 11.2, 5.65 and 1.32 MPa, from top to bottom, respectively.

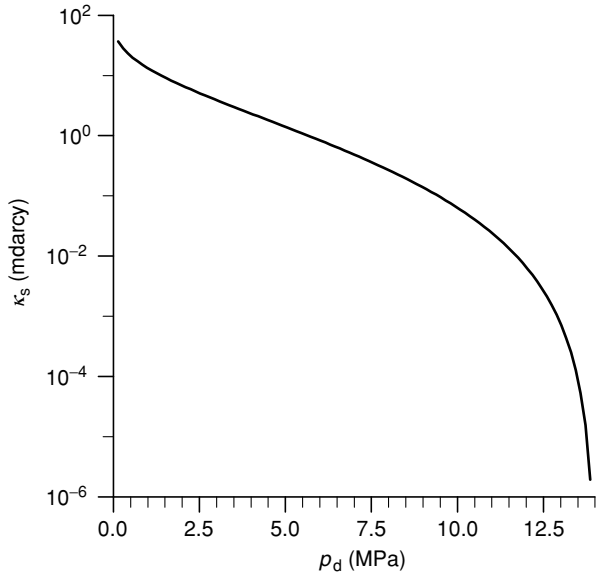

Figure 6 Frame permeability versus differential pressure.

$$K = \rho\left(V_P^2 - \frac{4}{3}V_S^2\right), \tag{27}$$

where $\rho = (1-\phi)\rho_s + \phi\rho_w$, and the porosity ϕ is given by MacKay *et al.* (1994). We consider a constant value of $\phi = 0.45$. Tobin *et al.* (1995) showed that for pore pressures less than 0.93 times the confining pressure, porosity changes are nearly insignificant, despite relative large variations in velocity.

We compute the dry-rock moduli by using Gassmann's equation:

$$K_{sm} = \frac{(\phi K_s/K_w + 1 - \phi)K - K_s}{\phi K_s/K_w + K/K_s - 1 - \phi} \tag{28}$$

(Carcione 2001, p. 225). The bulk moduli and density of quartz and water are given in Table 1. The lower value for μ_q with respect to pure quartz assumes that the sediments are clayey silts (Mavko *et al.* 1998, p. 307). Next, we consider the data points corresponding to zero pore pressure (overpressure ratio $\lambda = p/p_c = 0$), and fit those points with the following curve:

$$K_{sm}(p_c)\,[\text{GPa}] = 2.23 + 0.19p_c - 2.23\exp(-p_c/0.66), \tag{29}$$

where p_c is given in MPa. Equation (29) provides a better approximation than (7). The number of parameters is reduced in the case of calibration with log data, because direct measurements of pressure are not available in general.

Since we are dealing with sediments, which at zero confining pressure should not have any frame bulk modulus and rigidity, we obtain $K_{sm} = 0$ for $p_c = 0$. The dry-rock bulk modulus at zero pore pressure versus confining pressure is shown in Fig. 3 (solid line). The stars correspond to the dry-rock moduli obtained by using (28) and the experimental

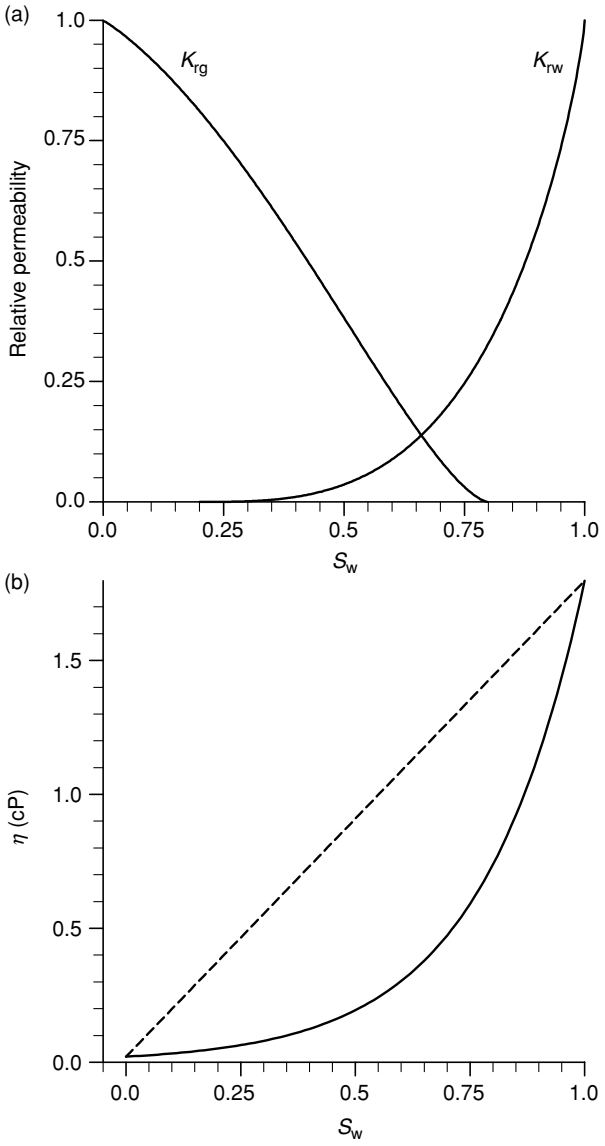

Figure 7 (a) Normalized relative permeabilities and (b) viscosity of the water/gas mixture as a function of water saturation. The dashed line is the linear viscosity law.

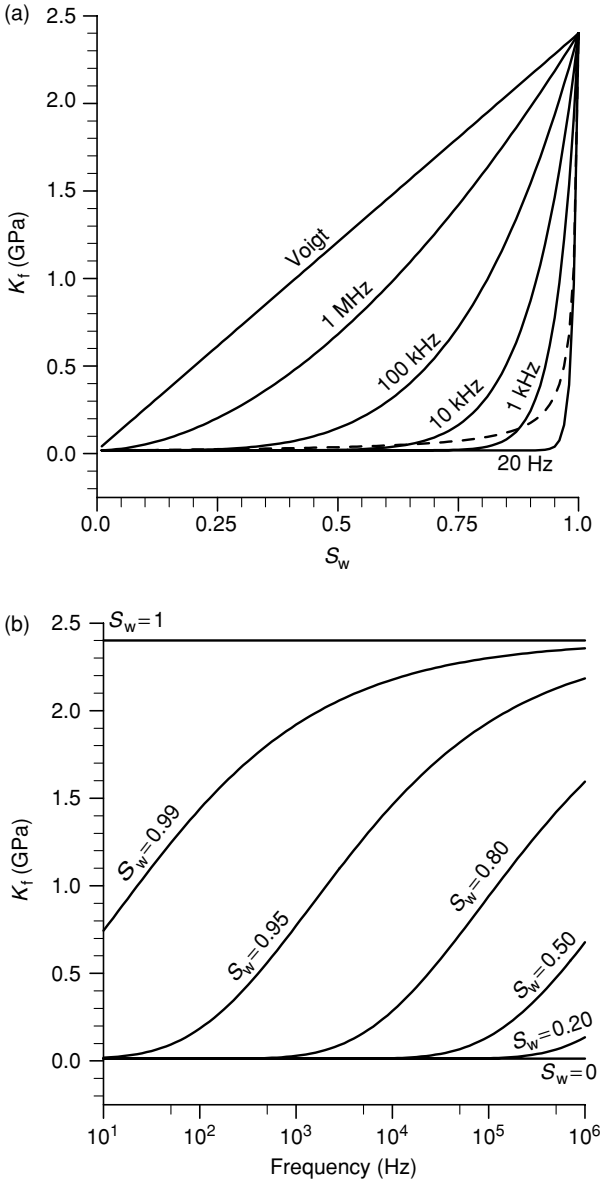

Figure 8 Bulk modulus of the water/gas mixture versus (a) water saturation and (b) frequency. The dashed line is Wood's modulus.

data of Tobin *et al.* (1995). As the confining pressure increases, the medium becomes load-bearing with a frame that develops rigidity. At this point, the effective stress becomes non-zero and the medium becomes rocklike in its behaviour. At zero confining pressure, both the bulk modulus and the rigidity modulus are zero.

In order to obtain the effective pressure law, we have to calculate the effective stress coefficient n_K for each data point in Fig. 3. We assume that n_K depends on the differential pressure $p_d = p_c - p$. Gangi and Carlson (1996) and Prasad and Manghnani (1997) showed that n for P-wave velocity is approximately linearly dependent on the differential pressure. The value of n_K for each point is obtained as follows. Assume that the pressure pair (p_c, p) is associated with each data point. The existence of an effective pressure law implies $K_{sm}(p_c, p=0) = K_{sm}\ (p_e = p_e - n_K p)$. Then, from (29), $n_K = (p_c - p_{c0})/p$, where p_{c0} is given by the intersection of the zero pore-pressure curve with a horizontal line passing through the point (p_c, p). The effective stress coefficients and an exponential fit (solid line),

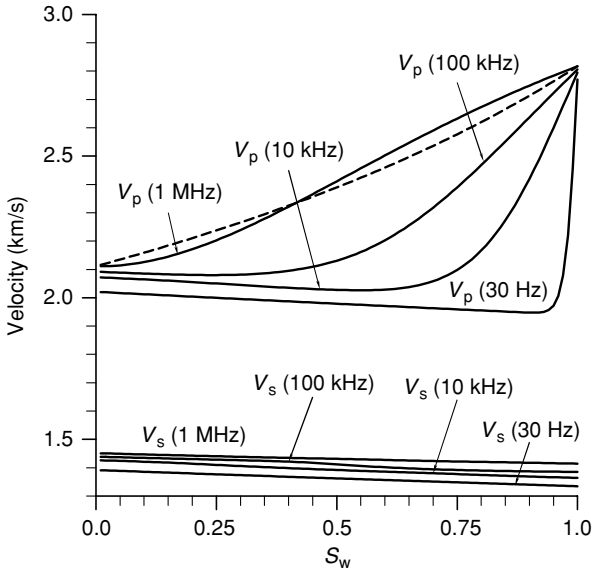

Figure 9 P- and S-wave velocities versus water saturation at different frequencies. The other saturating fluid is free gas and the gas-hydrate fraction is 0.3. Also shown, the P-wave velocity obtained by using Hill's equation (dashed line).

$$n_K = 0.89\exp(-0.43p_d),$$

are represented in Fig. 4(a) (p_d is given in MPa). It is clear that for sediments, the dependence on differential pressure is not linear. Figure 4(b) shows the dry-rock bulk modulus versus the effective pressure. To obtain the effective pressure law, we fit the data points in Fig. 4(b); the result is the solid line shown in the figure and represented by the curve:

$$K_{sm}(p_e)\,[\text{GPa}] = 1.73 + 0.23p_e - 1.7\exp(-p_e/0.17), \qquad (30)$$

where p_e is given in MPa. Similarly, we obtain the following expression for the dry-rock shear modulus:

$$\mu_{sm}(p_e)\,[\text{GPa}] = 0.54 + 0.06p_e - 0.54\exp(-p_e/0.12). \qquad (31)$$

To obtain the wet-rock moduli and the P-wave velocity, we use Gassmann's equation,

$$K = \frac{K_s - K_m + \phi K_m(K_s/K_w - 1)}{1 - \phi - K_m/K_s + \phi K_s/K_w} \qquad (32)$$

(Carcione 2001, p. 225) and the above relationship between V_P and V_S (see (26)). With regard to the rigidity modulus, we compute the wet-rock μ using Hamilton's (1979) V_S values. Then, we fit the zero pore-pressure curve (since $\mu_{sm} = \mu$ according to Biot's (1962) theory), and obtain the effective stress coefficient as before. Figure 5 shows the original data points (Tobin *et al.* 1995) and the P-wave velocities versus the overpressure ratio obtained with the effective pressure law.

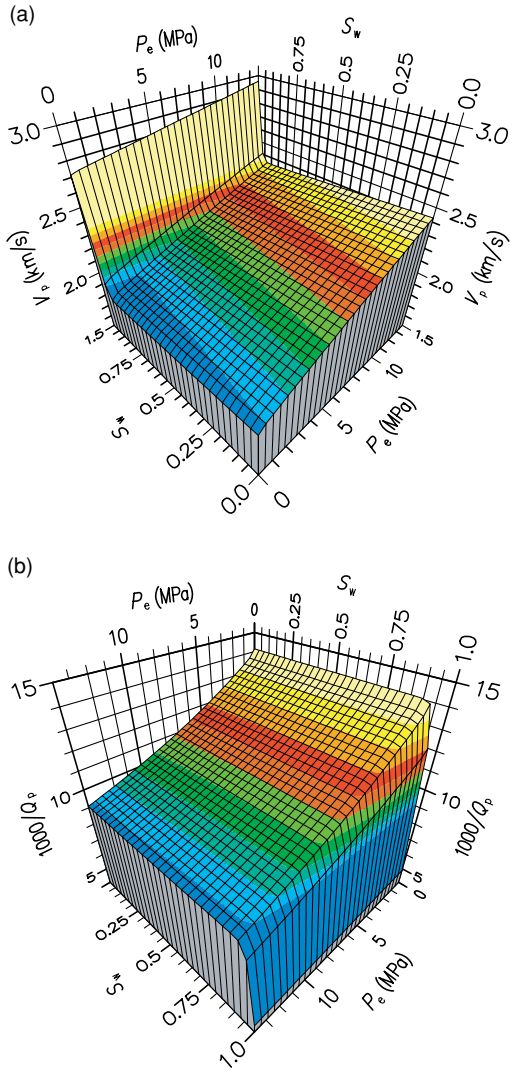

Figure 10 Three-dimensional plots of (a) the P-wave velocity and (b) the dissipation factor versus effective pressure and water saturation. The gas-hydrate fraction is 0.3 and the frequency is 30 Hz.

We now consider the rock containing gas hydrate, saturated with water and gas, and use the three-phase theory to compute its acoustic properties. Table 1 shows the properties of the different constituents. The values for the gas properties correspond to the depth of the BSR of site 892 (hydrostatic pore pressure). These properties were obtained using the van der Waals equation (see Section 5). (Depth is 70 m, $T = 8.9\,^{\circ}$C and $p = 8.3$ MPa.) The frame moduli K_{hm} and μ_{hm} are calculated using the equations given in Appendix A of Carcione and Tinivella (2000) (K_{im} and μ_{im}, respectively); the residual saturations are $S_{wg} = 0.2$ and $S_{gw} = 0.2$; the reference frequency in Brie *et al.*'s (1995) equation is $f_0 = 5.46$ MHz; the

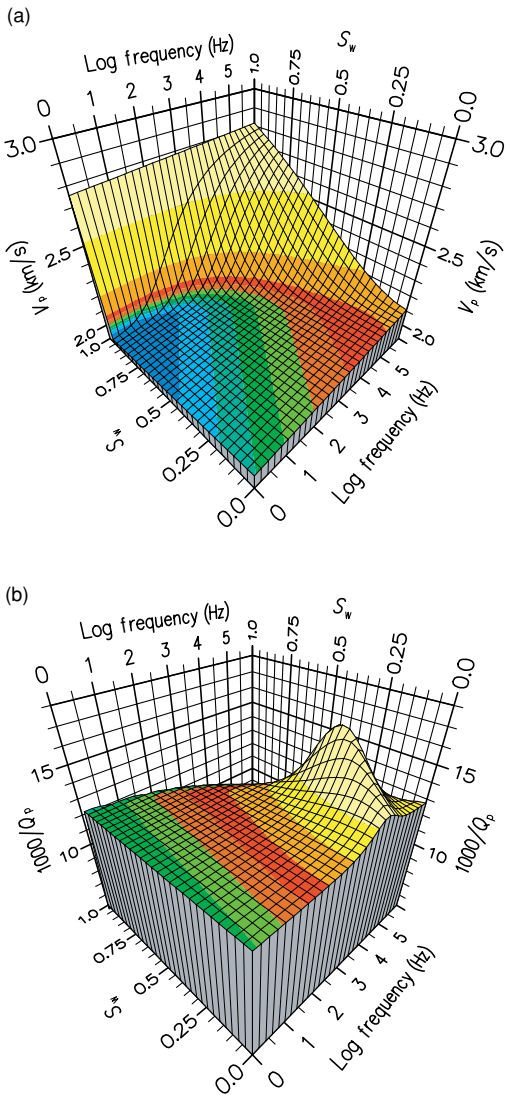

Figure 11 Three-dimensional plots of (a) the P-wave velocity and (b) the dissipation factor versus water saturation and frequency. The gas-hydrate fraction is 0.3, and the differential pressure is 0.6 MPa.

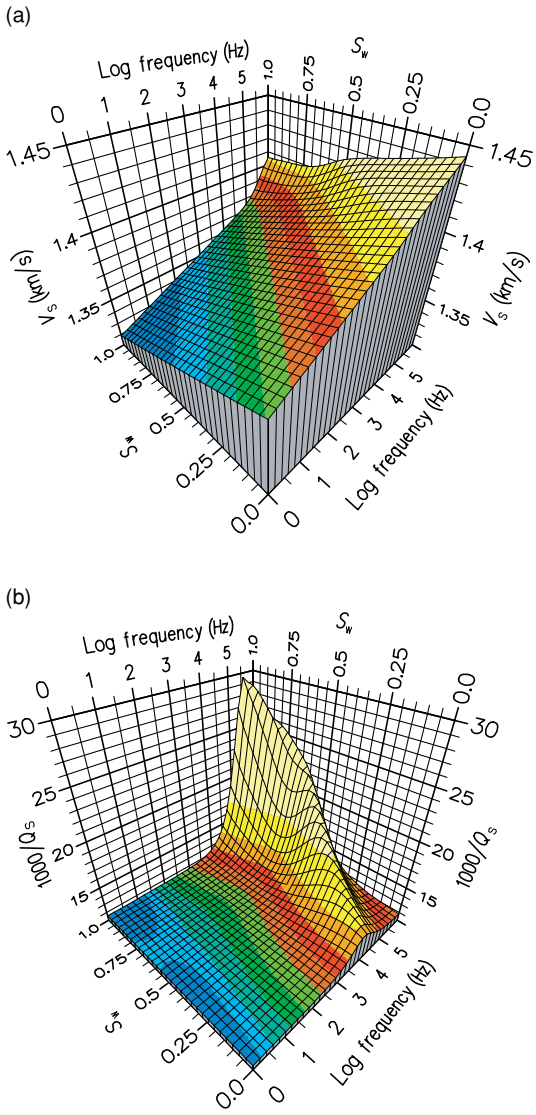

Figure 12 Same properties as in Fig. 11 but for S-waves.

permeabilities are $\kappa_{s0} = 10^{-13}\,\mathrm{m}^2 = 100\,\mathrm{mdarcy}$ (Moran, Gray and Jarrett 1995) and $\kappa_{i0} = 5 \times 10^{-4}\,\mathrm{m}^2$ (Leclaire *et al.* 1994); the relative permeability parameters are $m_w = 0.8$ and $m_g = 1.8$ (Van Genuchten 1978); the loss parameters are $Q_0 = 60$ and $\omega_0 = 2\pi$ MHz (assumed); $p_1 = 14$ MPa; $m = 0.26$ (Gangi 1981); and the parameters describing the shape of the pore network are $\xi_1 = \xi_3 = 8$ (Johnson *et al.* 1987).

Let us consider $\phi_h = 0.3$ and $S_w = 1$ (i.e. $\phi_w = 0.15$ and $\phi_g = 0$). Figure 6 shows the permeability versus differential pressure. The normalized relative permeabilities (a) and the viscosity of the water/gas mixture (b) are shown in Fig. 7 as a function of water saturation. Both permeabilities decrease for decreasing saturation of the corresponding fluid. In particular, there is practically no water flow below 50% water saturation. Figure 7(b) compares the linear mixing law (dashed line) with the more realistic mixing law of Teja and Rice (1981a,b) (continuous line). The linear relationship overestimates the viscosity of the mixture. Figure 8 shows the bulk modulus of the water/gas mixture versus water saturation (a) and frequency (b). Brie *et al.*'s (1995) model is in good agreement with Wood's bound at 20 Hz (dashed line).

Figure 9 shows the P- and S-wave velocities predicted by our model. The velocities are represented for several frequencies, from the seismic to the ultrasonic band. Also shown are the

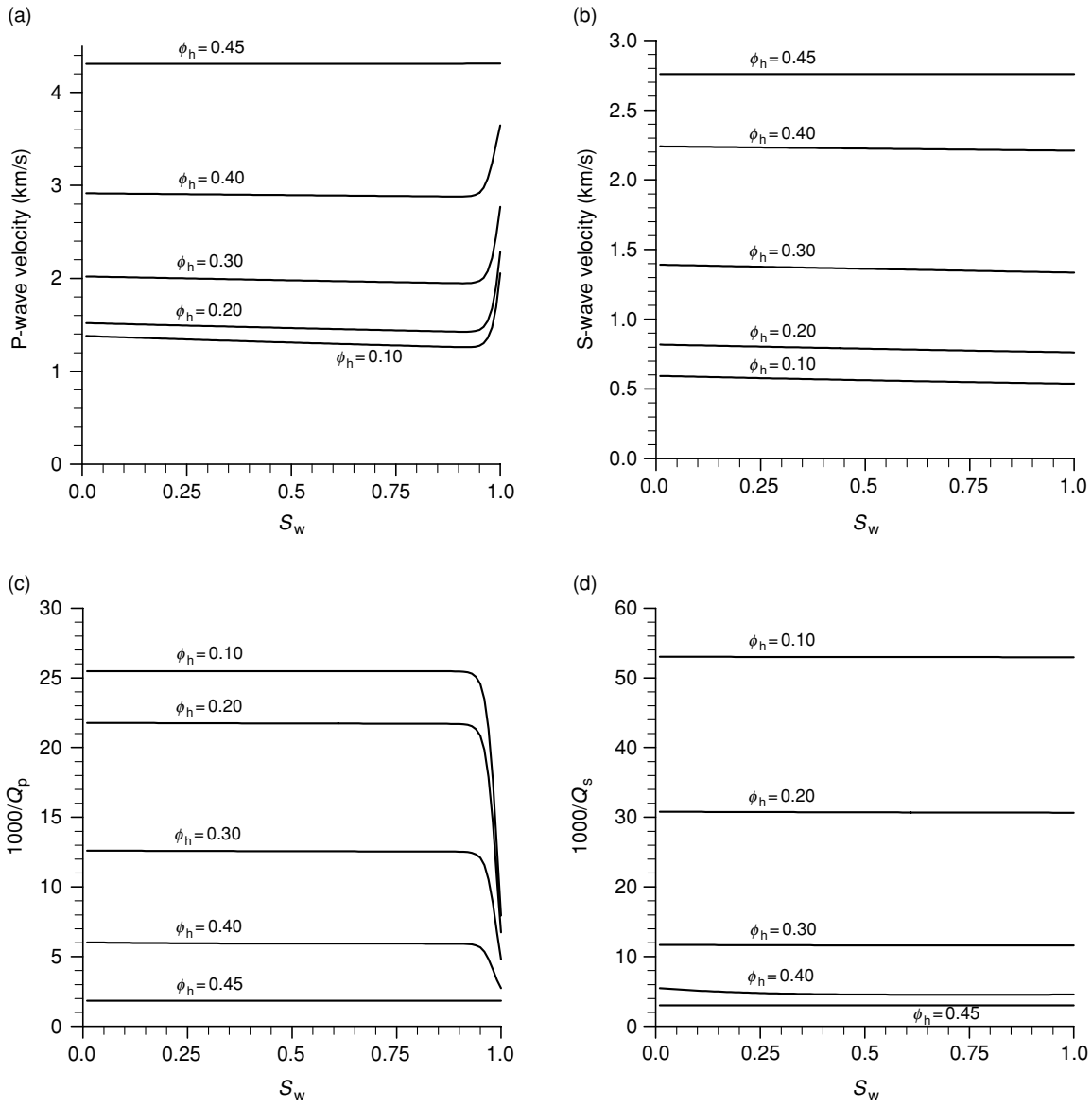

Figure 13 (a), (b) P- and S-wave velocities and (c), (d) dissipation factors versus water saturation for different values of the gas-hydrate fraction at a frequency of 30 Hz. The differential pressure is 0.6 MPa.

P-wave velocities obtained by using Hill's equation (dashed line, see Mavko *et al.* 1998, p. 115). In this case, we averaged the reciprocal of the P-wave modulus (ρV_P^2) at 1 MHz in the absence of attenuation. The reference frequency f_0 in Brie *et al.*'s (1995) equation was chosen to fit White's phase velocity (White 1975; Dutta and Odé 1979; Mavko *et al.* 1998, p. 207), using a diameter of 1 cm for the patches. (In this calculation, $\phi_h = 0$.) The use of Brie *et al.*'s (1995) model, though empirical, allowed us to model the acoustic properties of the sediment in the whole frequency range.

Three-dimensional plots of the P-wave velocity (a) and dissipation factor (b) versus effective pressure and water saturation are shown in Fig. 10. The gas-hydrate fraction is 0.3 and the frequency is 30 Hz. Note the strong decrease in the velocity and Q-factor with decreasing effective pressure. This effect is due mainly to the fact that the dry-rock moduli are sensitive functions of the effective pressure. (At very low effective pressures, the rock becomes unconsolidated.)

Figure 11 shows the same properties as in Fig. 10, but versus water saturation and frequency. In this case, the

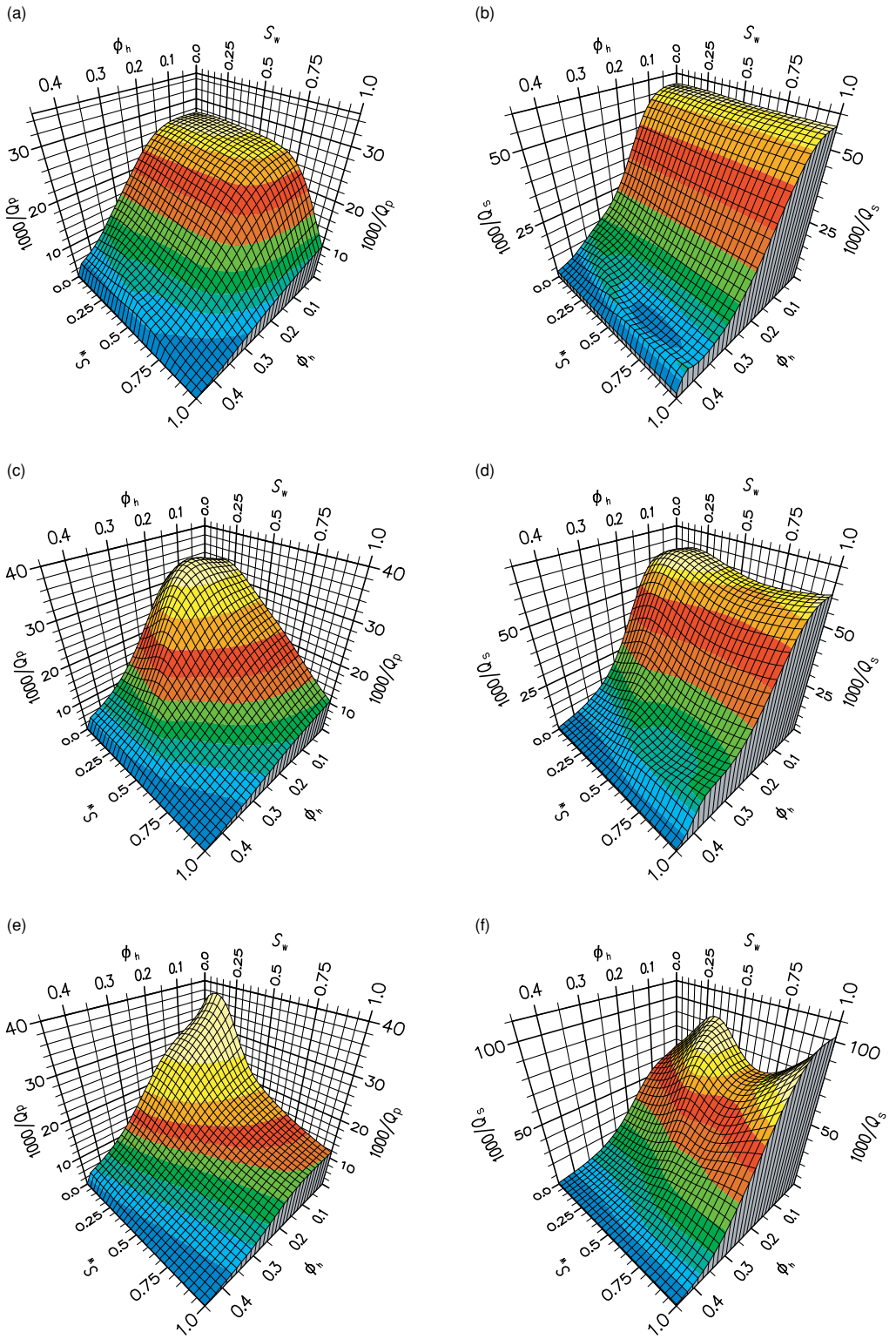

Figure 14 Three-dimensional plots of the dissipation factors versus water saturation S_w and gas-hydrate fraction ϕ_h for 10 kHz (a and b), 100 kHz (c and d) and 1 MHz (e and f). The differential pressure is 0.6 MPa.

differential pressure is 0.6 MPa and the effective pressure is 3.2 MPa ($p_c = 8.9$ MPa and $p = 8.3$ MPa). Figure 11(b) agrees qualitatively with a similar plot – based on experimental data of Massilon sandstone – published by Murphy (1982). The dissipation factor has a maximum value at the Biot relaxation peak, ranging from sonic frequencies for gas ($S_w = 0$) to ultrasonic frequencies for water-saturated rock with a peak value around $S_w = 0.4$. The latter behaviour agrees qualitatively with experimental data published by Yin, Batzle and Smith (1992).

The S-wave velocity and S-wave dissipation factor as functions of saturation and frequency are shown in Figs 12(a) and 12(b), respectively. The S-wave velocity increases with frequency and, generally, with decreasing water saturation. Attenuation has a maximum at approximately the location of the Biot peak (at constant water saturation) and 100% water saturation.

Figure 13 shows the wave velocities (a and b) and dissipation factors (c and d) versus water saturation and different values of the gas-hydrate fraction at 30 Hz. In general, velocity increases and attenuation decreases with increasing gas-hydrate concentration. Finally, the three-dimensional plots shown in Fig. 14 display more clearly the effect of gas hydrate and saturation on the dissipation factors for frequencies of 10 kHz (a and b), 100 kHz (c and d) and 1 MHz (e and f). Attenuation decreases with increasing gas-hydrate concentration, and for low concentrations the P-wave attenuation has a peak at nearly $S_w = 0.25$.

9 CONCLUSIONS

We have developed a model of the acoustic properties – wave velocity and attenuation – of sediments containing gas hydrate, free gas and water as a function of gas-hydrate concentration, pore pressure, temperature, frequency and partial saturation. The theory includes poro-viscoelasticity and viscodynamic effects to model the realistic attenuation values observed in rocks from low to high frequencies. The dry-rock moduli as a function of effective pressure are obtained from data of the Cascadia margin. The model predicts the behaviour of real sediments in many respects. For instance: (i) wave velocity increases considerably at high frequencies compared with low frequencies (at low frequencies, the fluid has enough time to achieve pressure equilibration, while at high frequencies, the fluid cannot relax and the bulk and shear moduli are stiffer than at low frequencies); (ii) there is a strong decrease in the velocity and Q-factor with decreasing effective pressure (this effect is due mainly to the fact that the dry-rock moduli are sensitive functions of the effective pressure); (iii) the dissipation factor has a maximum value at the Biot relaxation peak, ranging from sonic frequencies for gas to ultrasonic frequencies with a peak value around 40% water saturation; and (iv) in general, velocity increases and attenuation decreases with increasing gas-hydrate concentration.

Moreover, we have obtained the depth of the BSR as a function of the thermal conditions and sea-floor depth, by using Peltzer and Brewer's (2000) fit of Dickens and Quinby-Hunt's (1994) data. The depth of the BSR is lower for lower geothermal gradients, and increases with increasing depth and decreasing temperature of the sea floor.

ACKNOWLEDGEMENTS

This work was in part supported by the European Union under the project HYDRATECH 'Techniques for the Quantification of Methane Hydrate in European Continental Margins'. The authors are grateful to three anonymous reviewers for their valuable comments and suggestions.

REFERENCES

Andreassen K., Hogstad K. and Berteussen K.A. 1990. Gas hydrate in the southern Barents Sea indicated by a shallow seismic anomaly. *First Break* **8**, 235–245.

Bear J. and Bachmar Y. 1990. *Introduction to Modeling of Transport Phenomena in Porous Media*. Kluwer Academic Publishers.

Behrmann J.H. *et al.* 1992. *Proceedings ODP Initial Reports* **141**.

Berryman J.G. 1992. Effective stress for transport properties of inhomogeneous porous rock. *Journal of Geophysical Research* **97**, 17409–17424.

Biot M.A. 1962. Mechanics of deformation and acoustic propagation in porous media. *Journal of Applied Physics* **33**, 1482–1498.

Bland D.R. 1960. *The Theory of Linear Viscoelasticity.* Pergamon Press, Inc.

Brie A., Pampur, F., Marsala A.F. and Meazza O. 1995. Shear sonic interpretation in gas-bearing sands. SPE Annual Technical Conference, #30595, 701–710.

Brown K.M. and Bangs N.L. 1995. Thermal regime of the Chile triple junction: constraints provided by downhole temperature measurements and distribution of gas hydrates. *Proceedings ODP Initial Reports* **141**, 259–275.

Cadoret T., Marion D. and Zinszner B. 1995. Influence of frequency and fluid distribution on elastic wave velocities in partially saturated limestones. *Journal of Geophysical Research* **100**, 9789–9803.

Carcione J.M. 2001. Wave fields in real media: wave propagation in anisotropic, anelastic and porous media. In: *Handbook of Geophysical Exploration*, Vol. 31. Pergamon Press, Inc.

Carcione J.M., Cavallini F., Mainardi F. and Hanyga A. 2002. Time-domain seismic modeling of constant Q-wave propagation using fractional derivatives. *PAGEOPH* **159**(7), 1719–1736.

Carcione J.M. and Gangi A. 2000a. Non-equilibrium compaction and abnormal pore-fluid pressures: effects on seismic attributes. *Geophysical Prospecting* **48**, 521–537.

Carcione J.M. and Gangi A. 2000b. Gas generation and overpressure: effects on seismic attributes. *Geophysics* **65**, 1769–1779.

Carcione J.M. and Tinivella U. 2000. Bottom simulating reflectors: seismic velocities and AVO effects. *Geophysics* **65**, 54–67. Errata: 2001, **66**, 984.

Coyner K.B. 1984. *Effects of stress, pore pressure, and pore fluids on bulk strain, velocity, and permeability of rocks*. PhD thesis, MIT, Cambridge.

Davis E.E., Becker K., Wang K. and Carson B. 1995. Long-term observations of pressure and temperature in hole 892B, Cascadia accretionary prism. *Proceedings ODP Scientific Results* **146**, 299–311.

Dickens G.R. and Quinby-Hunt M.S. 1994. Methane hydrate stability in seawater. *Geophysical Research Letters* **21**(19), 2115–2118.

Dutta N.C. and Odé H. 1979. Attenuation and dispersion of compressional waves in fluid-filled porous rocks with partial gas saturation (White model) – Part I: Biot theory, Part II: Results. *Geophysics* **44**, 1777–1805.

Dvorkin J., Moos D., Packwood J.L. and Nur A. 1999. Identifying patchy saturation from well logs. *Geophysics* **64**, 1756–1759.

Fofonoff N.P. and Millard R.C. 1982. Algorithms for computation of fundamental properties of seawater. *UNESCO Technical Papers in Marine Science* **44**, 25–28.

Gangi A. 1981. The variation of mechanical and transport properties of cracked rock with pressure. In: *Rock Mechanics from Research to Application* (ed. H.H. Einstein), *Proceedings of the 22nd US Symposium on Rock Mechanics*, pp. 85–89.

Gangi A.F. and Carlson R.L. 1996. An asperity-deformation model for effective pressure. *Tectonophysics* **256**, 241–251.

Goldberg I. and Gurevich B. 1998. A semi-empirical velocity–porosity–clay model for petrophysical interpretation of P- and S-velocities. *Geophysical Prospecting* **46**, 271–285.

Grevemeyer I. and Villinger H. 2001. Gas hydrate stability and the assessment of heat flow through continental margins. *Geophysical Journal International* **145**, 647–660.

Guerin G. and Goldberg D. 2002. Sonic waveform attenuation in gas hydrate-bearing sediments from the Mallik 2L-38 research well, Mackenzie Delta, Canada. *Journal of Geophysical Research* **107**(B5), 10.1029/2001JB000556.

Guerin G., Goldberg D. and Meltser A. 1999. Characterization of in situ elastic properties of gas hydrate-bearing sediments on the Blake Ridge. *Journal of Geophysical Research* **104**(B8), 17781–17795.

Hamilton E.L. 1979. V_P/V_S and Poisson's ratios in marine sediments and rocks. *Journal of the Acoustical Society of America* **66**, 1033–1101.

Hashin Z. and Shtrikman S. 1963. A variational approach to the elastic behaviour of multiphase materials. *Journal of the Mechanics and Physics of Solids* **11**, 127–140.

Helgerud M.B., Dvorkin J., Nur A., Sakai A. and Collett T. 1999. Elastic-wave velocity in marine sediments with gas hydrates: effective medium modeling. *Geophysical Research Letters* **26**(13), 2021–2024.

Johnson D.L. 2001. Theory of frequency dependent acoustics in patchy-saturated porous media. *Journal of the Acoustical Society of America* **110**, 682–694.

Johnson D.L., Koplik J. and Dashen R. 1987. Theory of dynamic permeability and tortuosity in fluid-saturated porous media. *Journal of Fluid Mechanics* **176**, 379–402.

Kjartansson E. 1979. Constant (Q)-wave propagation and attenuation. *Journal of Geophysical Research* **84**, 4737–4748.

Knight R. and Dvorkin J. 1992. Seismic and electrical properties of sandstones at low saturations. *Journal of Geophysical Research* **97**, 17425–17432.

Krief M., Garat J., Stellingwerff J. and Ventre J. 1990. A petrophysical interpretation using the velocities of P and S waves (full waveform sonic). *The Log Analyst* **31**, 355–369.

Leclaire Ph., Cohen-Ténoudji F. and Aguirre-Puente J. 1994. Extension of Biot's theory of wave propagation to frozen porous media. *Journal of the Acoustical Society of America* **96**, 3753–3768.

Luo X. and Vasseur G. 1996. Geopressuring mechanism of organic matter cracking: numerical modeling. *AAPG Bulletin* **80**, 856–874.

MacKay M.E., Jarrad R.D., Westbrook G.K., Hyndman R.D. and Shipboard Scientific Party of ODP Leg 146. 1994. Origin of bottom-simulating reflectors: geophysical evidence from the Cascadia accretionary prism. *Geology* **22**, 459–462.

Mavko G., Mukerji T. and Dvorkin J. 1998. *The Rock Physics Handbook: Tools for Seismic Analysis in Porous Media*. Cambridge University Press.

McCann C. 1969. Compressional wave attenuation in concentrated clay suspensions. *Acustica* **22**, 352–356.

Moran K., Gray W.G.D. and Jarrett C.A. 1995. Permeability and stress history of sediment from the Cascadia margin. In: *Proceedings of the Ocean Drilling Program, Scientific Results* (eds B. Carson, G.K. Westbrook, R.J. Musgrave and E. Suess) **146**(1), 275–279.

Murphy W.F. 1982. Effect of partial water saturation on attenuation of Massilon sandstone and Vycor porous glass. *Journal of the Acoustical Society of America* **71**, 1458–1468.

Paull C.K., Matsumoto R., Wallace P. and Leg 164 Science Party. 1996. *Proceedings of the Ocean Drilling Program, Initial Reports*, Vol. 164. Ocean Drilling Program, College Station, TX.

Peltzer E.T. and Brewer P.G. 2000. Practical physical chemistry and empirical predictions of methane hydrate stability. In: *Natural Gas Hydrate in Oceanic and Permafrost Environments* (ed. M.D. Max), pp. 17–28.

Prasad M. and Manghnani M.H. 1997. Effects of pore and differential pressure on compressional wave velocity and quality factor in Berea and Michigan sandstones. *Geophysics* **62**, 1163–1176.

Scott-Blair G.W. 1949. *Survey of General and Applied Rheology*. Pitman.

Suess E. *et al.* 1988. *Proceedings ODP Initial Reports* **112**.

Taira A. *et al.* 1991. *Proceedings ODP Initial Reports* **131**.

Teja A.S. and Rice P. 1981a. Generalized corresponding states method for viscosities of liquid mixtures. *Indian Engineering and Chemistry Fundamentals* **20**, 77–81.

Teja A.S. and Rice P. 1981b. The measurement and prediction of the viscosities of some binary liquid mixtures containing n-hexane. *Chemical Engineering Science* **36**, 7–10.

Tinivella U. and Carcione J.M. 2001. Estimation of gas-hydrate concentration and free-gas saturation from log and seismic data. *The Leading Edge* **20**(2), 200–203.

Tobin H.J., Moore J.C. and Moore G.F. 1995. Laboratory measurement of velocity vs. effective stress in thrust faults of the Oregon accretionary prism: implications for fault zone overpressure. In: *Proceedings of the Ocean Drilling Program, Scientific Results* (eds B. Carson, G.K. Westbrook, R.J. Musgrave and E. Suess) **146**(1), pp. 349–358.

Urick R.J. 1948. Absorption of sound in suspensions of irregular particles. *Journal of the Acoustical Society of America* **20**, 283–289.

Van Genuchten M.T. 1978. *Calculating the unsaturated hydraulic conductivity with a closed form analytical model*. Report 78-WR-08, Princeton University, NJ.

Westbrook G.K. *et al.* 1994. *Proceedings ODP Initial Reports* **146**.

White J.E. 1975. Computed seismic speeds and attenuation in rocks with partial gas saturation. *Geophysics* **40**, 224–232.

Xu W. and Ruppel C. 1999. Predicting the occurrence, distribution and evolution of methane gas hydrate in porous marine sediments. *Journal of Geophysical Research* **104**(B3), 5081–5085.

Yin C.S., Batzle M.L. and Smith B.J. 1992. Effects of partial liquid/gas saturation on extensional wave attenuation in Berea sandstone. *Geophysical Research Letters* **19**, 1399–1402.

Zimmerman R.W. 1991. *Compressibility of Sandstones*. Elsevier Science Publishing Co.